Chemical Science

ROYAL SOCIETY OF CHEMISTRY

EDGE ARTICLE

View Article Online
View Journal | View Issue

Cite this: *Chem. Sci.*, 2025, **16**, 22621

All publication charges for this article have been paid for by the Royal Society of Chemistry

Gas-phase synthesis of naphthalene through an unconventional thermal alkyne–alkene [2 + 2] cycloaddition mechanism

Shane J. Goettl, †[a] Iakov A. Medvedkov,†[a] Anatoliy A. Nikolayev, †[b] Chao He, [a] Zhenghai Yang,[a] Alexander M. Mebel, *[c] Ankit Somani,[d] Adrian Portela-Gonzalez, [d] Wolfram Sander*[d] and Ralf I. Kaiser *[a]

Exotic cycloaddition entrance channels were discovered for the bimolecular gas-phase reactions of the phenylethynyl radical (C_6H_5CC, X^2A_1) with ethylene-d_4 (C_2D_4) and propylene (C_3H_6) as explored under single-collision conditions utilizing the crossed molecular beams technique combined with electronic structure and statistical calculations. Connecting the concepts of barrierless entrance channels, excited states, and facile non-photochemically activated cycloadditions, the reaction pathway features an unconventional thermal [2 + 2] cycloaddition forming a four-membered ring collision complex followed by multiple isomerizations prior to unimolecular decomposition *via* atomic hydrogen loss to (un)substituted naphthalenes—naphthalene-d_4 ($C_{10}H_4D_4$) and 1-/2-methylnaphthalene ($C_{11}H_{10}$). The small energy gap between the singly-occupied a_1 highest occupied molecular orbital (HOMO) with a σ-character and the underlying doubly-occupied b_1 molecular orbital with a π-character allows a facile promotion of an electron. This in turn enables a versatile low-temperature reactivity of phenylethynyl, where the end-on and side-on barrierless approaches of ethylene are due to its interaction with the σ and π orbitals, respectively, thus suggesting this mechanism as a possible method for tuning substituents in polycyclic aromatic hydrocarbon (PAH) formation and highlighting its versatility as a probe of fundamental carbon chemistry *via* counterintuitive cycloaddition reactions under single-collision conditions.

Received 8th August 2025
Accepted 22nd October 2025

DOI: 10.1039/d5sc05991g

rsc.li/chemical-science

Introduction

For more than half a century, cycloaddition reactions—chemical reactions forming a cyclic adduct from two unsaturated molecules or unsaturated moieties within the same molecule—have played a fundamental role in advancing organic synthetic chemistry,[1] materials science,[2] and biochemistry[3] in the realms of catalysis,[4–6] polymer synthesis,[7,8] and supramolecular chemistry in the bottom-up synthesis of fullerenes.[9,10] The iconic [4 + 2] Diels–Alder reaction is central to the understanding of reactions between a diene and an olefin to facilitate formation of a six-membered ring under thermal conditions.[11] Conversely, as a direct consequence of orbital symmetry,[12] the [2 + 2] cycloaddition requires photochemical activation[13] or a catalyst[14] to prepare a four-membered ring. Concerted thermal [2 + 2] reactions are rare[15] and involve activated olefins such as allenes or ketenes. Ketenes, unlike alkenes, can align antarafacially with respect to the alkene reactant. Thus, a suprafacial-antarafacial geometry is required for concerted, thermal [2 + 2] cycloadditions to proceed (Fig. 1).[16]

Whereas a mechanistic understanding of the role of the orbital symmetry in cycloadditions of closed shell reactants has emerged, alkenyl radicals have been scarcely associated with cycloaddition reactions, with few examples as intramolecular radical addition,[17] diradical addition, and sequential addition and cyclization *via* recombination (Fig. 1).[18] Traditionally, olefinic or acetylenic hydrocarbon radicals in their doublet ground states are connected with, *e.g.*, simple addition–elimination mechanisms such as bimolecular phenylethynyl ($C_6H_5CC^{\bullet}$; X^2A_1) radical reactions with allene (H_2CCCH_2) and methylacetylene (CH_3CCH) leading to chain extension and hence acyclic hydrocarbons under single collision conditions.[19] Therefore, cycloadditions of acetylenic radicals such as of phenylethynyl ($C_6H_5CC^{\bullet}$; X^2A_1) represent one of the least explored classes of reactions leading to molecular mass growth processes in physical organic chemistry, computational chemistry, combustion sciences, and astrophysics.

Herein, we provide a rare glimpse into the unexpected chemical dynamics initiated *via* [2 + 2] cycloaddition of the bimolecular gas-phase reactions of the phenylethynyl radical

[a]*Department of Chemistry, University of Hawai'i at Mānoa, Honolulu, HI 96822, USA. E-mail: ralfk@hawaii.edu*

[b]*Samara National Research University, Samara 443086, Russia*

[c]*Department of Chemistry and Biochemistry, Florida International University, Miami, FL 33199, USA. E-mail: mebela@fiu.edu*

[d]*Lehrstuhl für Organische Chemie II, Ruhr-Universität Bochum, 44801, Bochum, Germany. E-mail: wolfram.sander@rub.de*

† Contributed equally.

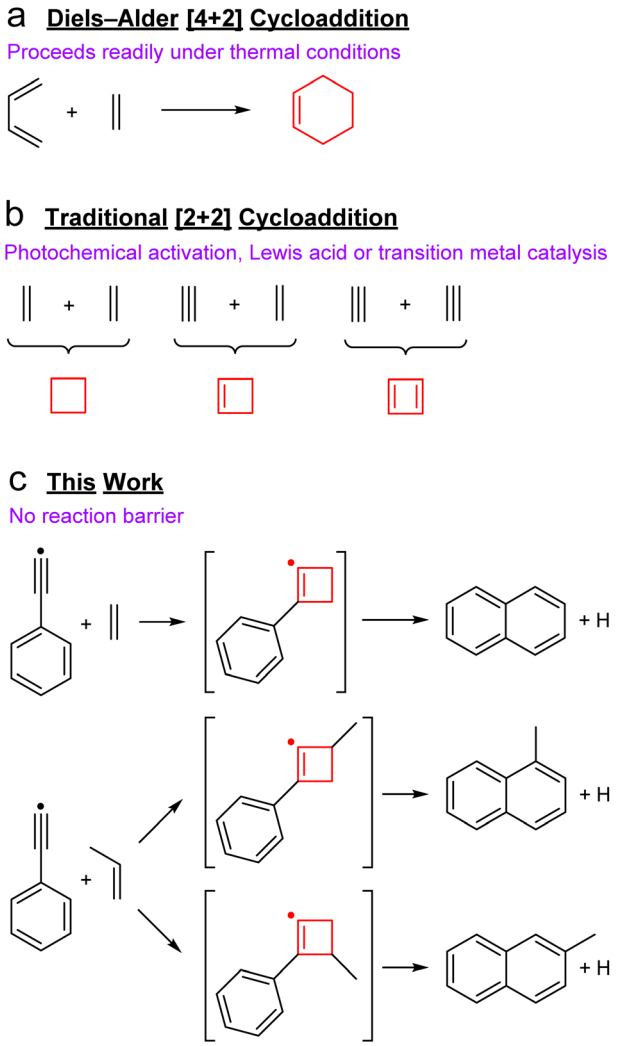

Fig. 1 Schematic reaction mechanisms leading to cyclic structures *via* the Diels–Alder reaction (a) and traditional [2 + 2] cycloaddition (b), as well as the findings of the current work (c).

($C_6H_5CC^{\bullet}$, X^2A_1) with ethylene-d_4 (C_2D_4) and propylene (C_3H_6) in the entrance channels under single-collision conditions. Combining the crossed molecular beams results with electronic structure and statistical calculations, this study affords compelling evidence on the gas-phase preparation of naphthalene-d_4 ($C_{10}H_4D_4$) and 1-/2-methylnaphthalene ($C_{11}H_{10}$) as prototype 10π aromatic systems. The consequence of the gas-phase synthesis of polycyclic aromatic hydrocarbons (PAHs) carrying two fused benzene rings is driven by unconventional non-concerted cycloaddition reactions in the entrance channels on the doublet surface leading to cyclobutene radical transients *via* a cyclic arrangement of the atoms along with a reorganization of σ and π bonds initiated by a single collision. These facile, barrierless [2 + 2] cycloadditions lead eventually to (substituted) naphthalenes and defy conventional wisdom that acetylenic radicals react *via* simple chain extension. This study showcases the capacity of crossed molecular beam experiments in conjunction with electronic structure calculations in unraveling reaction pathways to aromatic, multi-ringed structures.

Results and discussion

Laboratory frame: C_6H_5CC–C_2D_4 system

In the bimolecular reaction of the phenylethynyl radical ($C_6H_5CC^{\bullet}$, 101 amu) with ethylene-d_4 (C_2D_4, 32 amu), reactive scattering signal was observed at mass-to-charge ratios (m/z) of 132 ($C_{10}H_4D_4^+$, $^{13}C_{10}H_5D_3^+$) and 131 ($C_{10}H_5D_3^+$, $C_{10}H_3D_4^+$, $^{13}C_{10}H_4D_3^+$). The time-of-flight (TOF) spectra of these m/z values overlap after scaling (Fig. S3) indicating that signal at $m/z = 131$ arises from dissociative electron impact fragmentation of the $C_{10}H_4D_4$ parent in the electron impact ionizer (reaction (1a)). No signal was detected for the adduct at $m/z = 133$, and background intensity is too high at $m/z = 103$ ($C_8H_5D^+$) to scan for the deuterium abstraction pathway. Anyway, D abstraction is not expected to be a major reaction route since abstraction typically features a large entrance barrier, and the ethynyl radical (C_2H)—the simple prototype radical for phenylethynyl—reacts with unsaturated hydrocarbons predominantly by addition, not abstraction.[20,21] Therefore, at least the atomic hydrogen loss channel is open (reaction (1a)), while it cannot be unambiguously concluded whether atomic deuterium loss is present (reaction (1b), see SI for detail). The TOF spectra were then collected at distinct angles in the scattering plane for the parent ion at $m/z = 132$ in 5° increments on either side of the center-of-mass (CM) angle (Θ_{CM}) of 17.8° (Fig. 2b), with respect to the phenylethynyl beam ($\Theta = 0°$). These TOFs were integrated to obtain a laboratory angular distribution (LAD) (Fig. 2a). The TOF spectra are fairly narrow and range only from about 700 to 950 μs—reflected in a rather small LAD range of only 30°. Additionally, the LAD is symmetric with respect to the Θ_{CM}, which is indicative of indirect scattering dynamics involving $C_{10}H_5D_4$ intermediate(s)—since strongly forward or backward scattering would correlate to short-lived direct reactions—fragmenting eventually to $C_{10}H_4D_4$ product(s) plus atomic hydrogen (reaction (1a)).

Laboratory frame: C_6H_5CC–C_3H_6 system

Signal for the reaction of the phenylethynyl radical ($C_6H_5CC^{\bullet}$, 101 amu) with propylene (C_3H_6, 42 amu) was observed at $m/z = 142$ ($C_{11}H_{10}^+$). Like the phenylethynyl/ethylene-d_4 system, the TOFs were only about 250 μs wide (Fig. 2d). Data at $m/z = 142$ were collected at the CM angle of 22.3° in steps of 2.5°. The LAD (Fig. 2c) is nearly symmetric with respect to the Θ_{CM} to insinuate indirect reaction dynamics through $C_{11}H_{11}$ intermediate(s) leading to $C_{11}H_{10}$ product(s) plus atomic hydrogen (reaction (2)).

$$C_6H_5CC\ (101\ amu) + C_2D_4\ (32\ amu) \rightarrow C_{10}H_4D_4\ (132\ amu) + H\ (1\ amu) \quad (1a)$$

$$\rightarrow C_{10}H_5D_3\ (131\ amu) + D\ (2\ amu) \quad (1b)$$

$$C_6H_5CC\ (101\ amu) + C_3H_6\ (42\ amu) \rightarrow C_{11}H_{10}\ (142\ amu) + H\ (1\ amu) \quad (2)$$

Overall, the laboratory data provide compelling evidence on molecular mass growth processes *via* the phenylethynyl *versus*

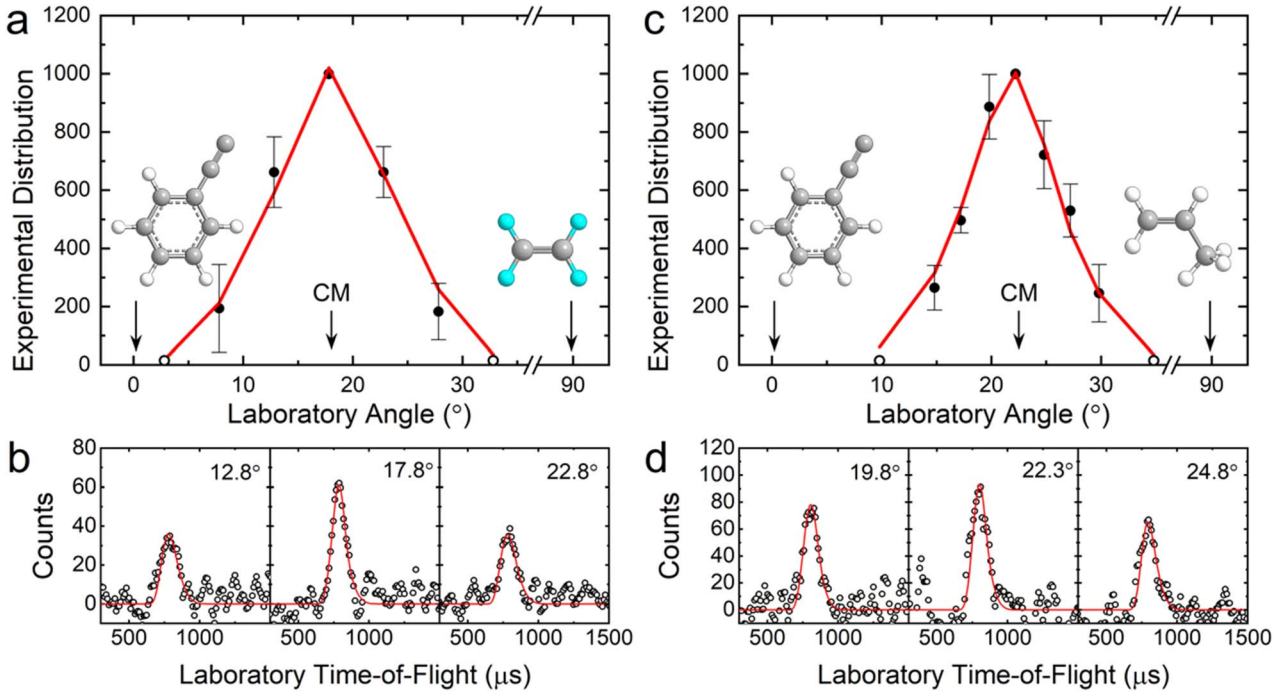

Fig. 2 Laboratory angular distributions (a and c) and time-of-flight (TOF) spectra (b and d) recorded at mass-to-charge (m/z) = 132 and 142 for the reactions of phenylethynyl (C_6H_5CC) with ethylene-d_4 (C_2D_4, a and b) and propylene (C_3H_6, c and d), respectively. CM represents the center-of-mass angle, and 0° and 90° define the directions of the phenylethynyl and ethylene-d_4/propylene beams, respectively. The black solid circles depict the data, black open circles represent simulated points, and red lines show the fits. Carbon atoms are colored gray, hydrogens are white, and deuteriums are light blue.

atomic hydrogen exchange pathways leading to products with the molecular formulas $C_{10}H_4D_4$ and $C_{11}H_{10}$, respectively.

Center-of-mass frame

With the detection of the $C_{10}H_4D_4$ and $C_{11}H_{10}$ isomer(s) *via* reactions (1a) and (2), respectively, information on the chemical dynamics of these reactions can be obtained by converting the laboratory data into the CM reference frame.[22] For both systems, the TOFs and LAD could be fit with a single reaction channel through atomic hydrogen loss with the products mass combinations of 132 amu/1 amu and 142 amu/1 amu, respectively. The best-fit CM functions, *i.e.* the product translational energy ($P(E_T)$) and angular ($T(\theta)$) flux distributions, are compiled in Fig. 3. Since the experiments utilize high-energy electron impact ionization, products are not detected isomer-selectively; however, the $P(E_T)$ is a valuable tool which can help to alleviate this limitation. For the phenylethynyl/ethylene-d_4 system, the $P(E_T)$ exhibits a maximum (E_{max}) at 347 ± 48 kJ mol^{-1} (Fig. 3a). For those molecules born without internal energy, the reaction energy ($\Delta_r G$) can be obtained through energy conservation with $\Delta_r G = E_C - E_{max}$, where E_C is the collision energy. This gives a reaction energy of −328 ± 49 kJ mol^{-1} for reaction (1a). While not exclusive of other, less exoergic channels, this method guarantees the existence of product(s) yielded at the specified reaction energy. Combining this information with known enthalpies of formation and/or electronic structure calculations for the reaction species can provide identification of the unique product isomer(s) formed. Additionally, the $P(E_T)$ features a distribution maximum at 45 kJ mol^{-1} indicating a tight exit transition state.[23] Second, the $T(\theta)$ contains details about the underlying reaction mechanism. In this case, the $T(\theta)$ is isotropic, *i.e.* it has equal intensity at all angles (Fig. 3b). This finding suggests indirect scattering dynamics through the formation of $C_{10}H_4D_4$ complex(es) with lifetimes longer than their rotational period(s), while short-lived and direct mechanisms would instead feature strong peaking near 0 or 180°. These results are also reflected in the product flux contour map, which represents the overall outcome of the reaction (Fig. 3c).

For the phenylethynyl/propylene system, the recovered reaction energy of −321 ± 58 kJ mol^{-1} and distribution maximum of the $P(E_T)$ of 34 kJ mol^{-1} (Fig. 3d) are similar to those for the phenylethynyl/ethylene-d_4 system. However, while the best-fit $T(\theta)$ shows intensity at all angles (Fig. 3e), this distribution reveals a maximum at 90°. This finding indicates geometrical constraints in the decomposition of the reaction intermediate with the hydrogen atom ejection occurring perpendicularly to the plane of the rotating and decomposing intermediate (Fig. 3f).[24]

Potential energy surfaces: C_6H_5CC–C_2D_4 system

In the case of polyatomic systems, it is beneficial to combine the experimental results with electronic structure and statistical calculations to reveal the reaction pathways and nature of the products. The potential energy surfaces (PESs) visualizing the intermediates, transition states, and products are shown in Fig. 4–6. Rice–Ramsperger–Kassel–Marcus (RRKM) theory[25] was

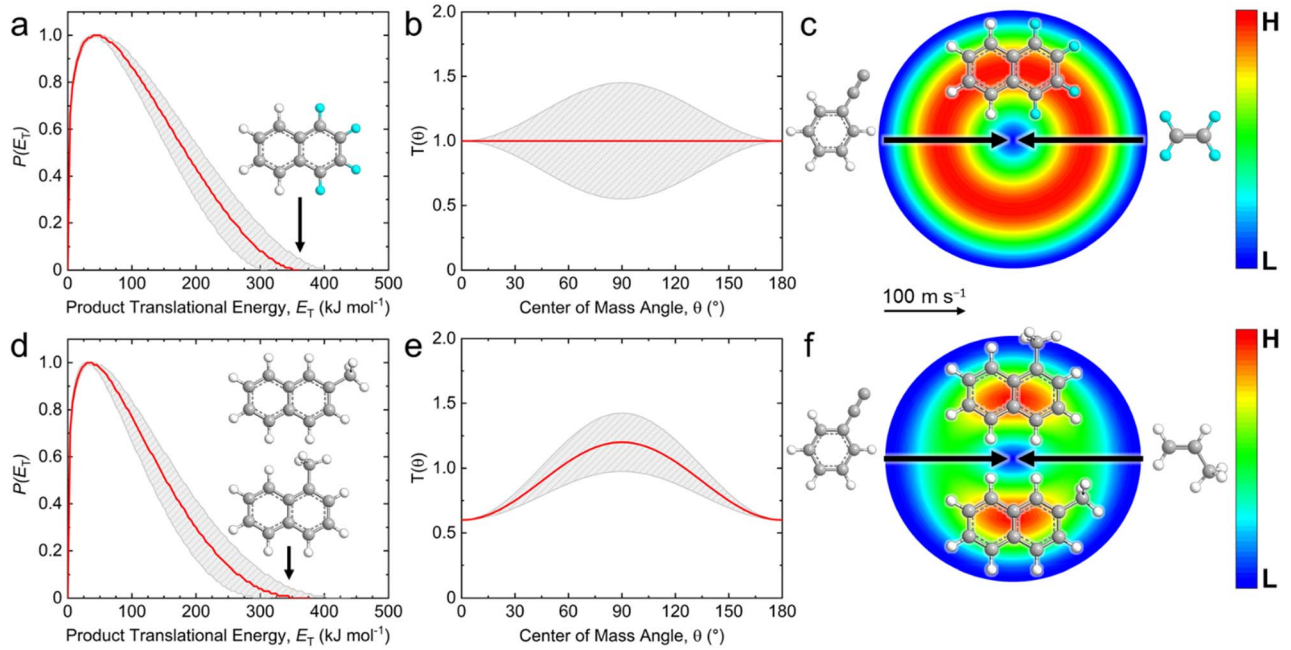

Fig. 3 Center-of-mass product translational energy (a and d) and angular (b and e) flux distributions, as well as the associated flux contour maps (c and f) leading to the formation of $C_{10}H_4D_4$ and $C_{11}H_{10}$ isomers in the reactions of phenylethynyl (C_6H_5CC) with ethylene-d_4 (C_2D_4, a–c) and propylene (C_3H_6, d–f). Red lines define the best-fit functions while shaded areas provide the error limits. The flux contour map represents the intensity of the reactively scattered products as a function of product velocity (u) and scattering angle (θ), and the color bar indicates flux gradient from high (H) to low (L) intensity.

utilized to calculate microcanonical rate constants $k(E)$. This method is viable since unimolecular reaction steps depend only on internal energies of the species involved, and the RRKM theory requirement that the internal vibrational energy be randomly distributed among all vibrational modes of the collision complex is consistent with the experimental determination of an indirect reaction with long-lived intermediates. These rate constants were used to calculate product branching ratios at various collision energies (Tables 1 and S1–S11). Looking first at reaction (1), the experimental reaction energy of -328 ± 49 kJ mol^{-1} matches the calculated energy for the formation of naphthalene ($C_{10}H_8$, **p1**) of -342 kJ mol^{-1} along with atomic hydrogen loss (Fig. 4). In fact, **p1** is the only H loss product which features a calculated reaction energy exoergic enough to fall within the error limits of the experimentally observed value. It is important to reiterate that hard ionization was used to detect products; as such, while we can specify the formation of product(s) corresponding to the maximum kinetic energy release (Fig. 3a and d), other products with lower exoergicity can also be formed but remain unidentified. From a traditional sense, the reaction of phenylethynyl radicals with ethylene should be initiated by barrierless addition of the radical center of phenylethynyl—located on the terminal carbon of the ethynyl group—to one of the carbons of ethylene forming a non-cyclic four-carbon chain moiety in the collision complex (**i1**) (Fig. 4a). Simple atomic hydrogen loss from the attacked carbon of the ethylene group leads over a 143 kJ mol^{-1} exit barrier to the formation of (but-3-en-1-yn-1-yl)benzene ($C_{10}H_8$, **p2**) exoergic by 118 kJ mol^{-1}. While the reaction energy to form **p2** is much lower than the experimentally observed value of -328 ± 49 kJ mol^{-1}, the kinetic energy release of **p2** formation may be cloaked within the lower energy portion of the $P(E_T)$. To get to the product which matches the experimental reaction energy (**p1**), collision complex **i1** must pass over a high barrier of 183 kJ mol^{-1} *via* [1,2]-H shift to form a butadienyl moiety on the side chain (intermediate **i2**). The reaction pathways continuing from **i2** involve a plethora of possible isomerization steps (Fig. S6), with the most energetically favorable route to naphthalene (**p1**) comprising bond rotation about the C2–C3 single bond of the side chain (**i2** → **i3**), [1,4]-H shift from the terminal carbon atom (**i3** → **i4**), three-membered ring closure (**i4** → **i7**) and reopening (**i7** → **i20**) of the three carbons at the end of the side chain, six-membered ring closure of the side chain (**i20** → **i22**), and finally hydrogen atom ejection (**i22** → **p1**). Nevertheless, the isomerization from **i1** to **i2** is energetically less favored by 40 kJ mol^{-1} than the addition–elimination channel (**i1** → **p2**), suggesting that **p2** formation should dominate. Thus, an alternate pathway to naphthalene is required to account for the experimental results.

Fig. 4b shows a PES featuring an additional, unconventional reaction entrance channel and reaction pathway. This route proceeds through an entrance channel in which the carbons in the ethynyl moiety of the phenylethynyl radical add nearly simultaneously *via* a non-concerted [2 + 2] cycloaddition to ethylene, forming a four-membered ring collision complex (**i25**) without barrier. This is followed by ring opening from the bond of the attacked ethylene moiety (**i25** → **i26**), [1,4]-hydrogen shift from the phenyl ring to the β-carbon of the side group chain (**i26**

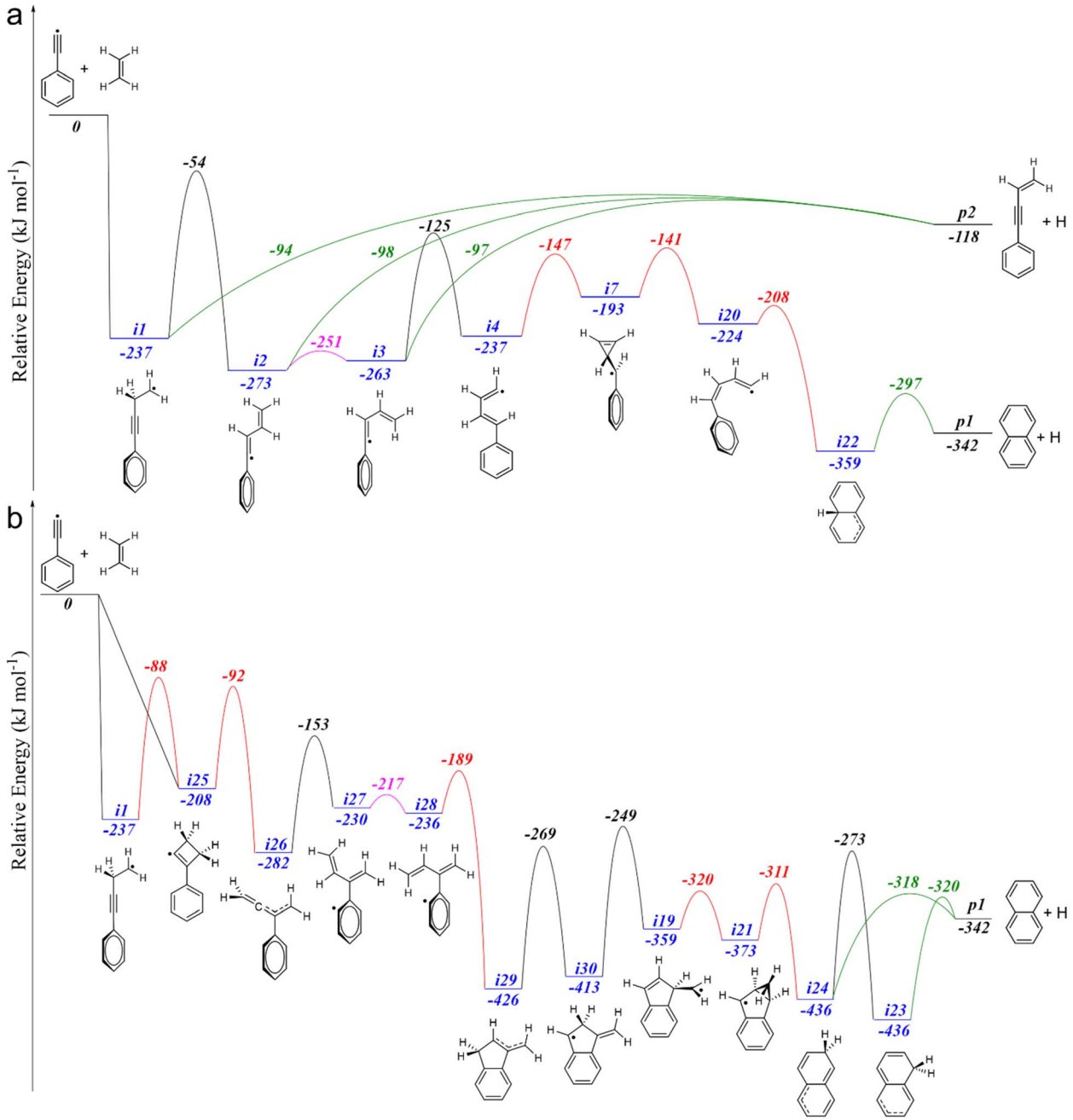

Fig. 4 Schematic potential energy surfaces leading to the formation of naphthalene ($C_{10}H_8$) from the reaction of the phenylethynyl radical (C_6H_5CC) with ethylene (C_2H_4) through two different pathways (a and b) calculated at the G3(MP2,CC)//ωB97X-D/6-311G(d,p) level. Hydrogen migration, bond rotation, and ring opening/closing are denoted by black, magenta, and red lines between intermediates, respectively, while exit channels to products are green. The complete surfaces are shown in Fig. S3–S8.

→ **i27**), rotation about the α–β carbon–carbon single bond (**i27** → **i28**), five-membered ring closure (**i28** → **i29**), additional hydrogen migrations (**i29** → **i30** → **i19**), three-membered ring closure (**i19** → **i21**) and opening (**i21** → **i24**), and finally hydrogen atom loss to form naphthalene (**i24** → **p1**). In order to have H loss in the ethylene-d_4 experiment, **i24** must undergo a [1,2]-deuterium shift to **i23** before hydrogen atom emission to **p1**. The highest barrier for this route is the first isomerization step at −92 kJ mol^{-1} (**i25** → **i26**) with respect to the separated reactants, whereas that for the traditional naphthalene formation pathway (**i1** → **i2**) in Fig. 4a is 54 kJ mol^{-1} below reactants. The lower barrier in the cycloaddition case is indicative of a more favorable route toward naphthalene from **i25** as compared to that from **i1**, which is reinforced by RRKM calculations. Statistical branching ratios for the formation of naphthalene from the traditional route (Fig. 4a) give values of less than 0.1% compared to other possible products (Table 1 and Fig. S4–S6), while those calculated for the cycloaddition route to

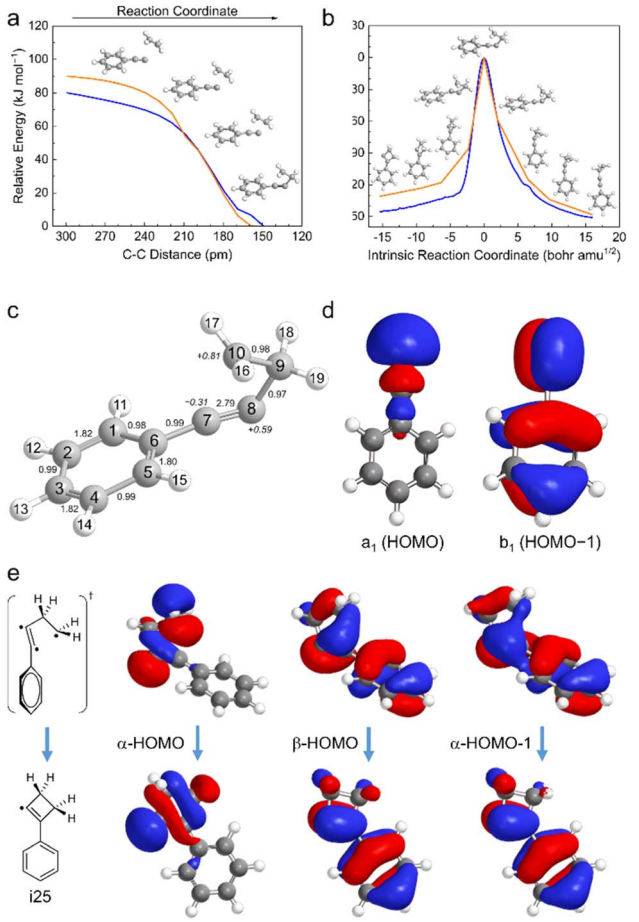

Fig. 5 Potential energy profiles for the side-on addition of ethylene to phenylethynyl (a) and from the initial transition state towards **i1** and **i25** (b) calculated at the ωB97X-D/6-311G(d,p) (blue curves) and G3(MP2,CC) (orange cuves) levels of theory. The structure of the transition state connecting **i1** and **i25** is highlighted with all carbon–carbon bond orders and select carbon atom spin densities (c). Panel (d) shows the singly-occupied HOMO and doubly-occupied HOMO−1 frontier orbitals for the phenylethynyl radical, while (e) presents the orbitals involved in the transformation of intermediate **i1** to **i25**. This sequence shows the formation of the new carbon–carbon bond during closing of the four-membered ring, consolidation of the radical on the left-hand-side carbon in the four-member ring, and the complete disappearance of the double-bond character in the ethylene fragment. This scheme also visualizes that the b_1 orbital of the phenylethynyl reactant (HOMO−1 in Fig. 5d), which becomes singly occupied in the reactant after an electron promotion to the excited state, is actively involved and becomes doubly occupied in the transition state connecting **i1** and **i25** and eventually in **i25**.

naphthalene predict an increased value from 3% with nominal computed relative energies to up to 14% at $E_C = 20$ kJ mol^{-1}—which is close to the experimental collision energy—when the relative energies are varied within the error limits of the computations. Interestingly, lower collision energies favor the formation of naphthalene and the margins of its computed yield increase to 4–18% at zero collision energy (Tables S4 and S5). Therefore, as a whole, this study provides evidence for the synthesis of naphthalene *via* the reaction of phenylethynyl radicals with ethylene through an unconventional [2 + 2] cycloaddition entrance channel. The remaining product fraction is accounted for by higher energy isomers outside the error range of the experimentally derived reaction energy (Tables S3–S5, Fig. S7 and S8) which are likely veiled within the lower kinetic energy release portion of the $P(E_T)$.

Can the [2 + 2] cycloaddition producing **i25** in the entrance channel compete with the classical addition to the radical site of phenylethynyl leading to **i1**? To address this question we scanned the minimal energy path (MEP) for the approach of ethylene toward the C≡C triple bond in the phenylethynyl radical sideways (Fig. 5). Parallel side-on symmetric addition of ethylene features a potential wall of 60 kJ mol^{-1}; no first-order saddle point exists. Therefore, the system follows the route in which the terminal carbon of the ethynyl moiety bonds with one of the ethylene carbon atoms. Here, the computed MEP shows a monotonic energy decrease from the reactants on the way to the transition state connecting **i25** and **i1** (see panels a and b in Fig. 5). Thus, it is predicted that the transition state region can be barrierlessly accessed in the entrance channel (Fig. 5a), after which the ensuing pathway can proceed in the directions of either ring opening to **i1** or ring closure toward **i25** (Fig. 5b). The assessment of the branching ratio between the formation of **i1** and **i25** in the reaction onset is a dynamics problem which in principle can be addressed by running trajectories at the initial stage of the phenylethynyl–ethylene bimolecular collisions to evaluate the statistics of the appearance of **i1** and **i25**, where production of the latter favors the ultimate formation of naphthalene. Interestingly, the wavefunction of the transition state between **i1** and **i25** can be characterized as a superposition of two Lewis structures, one with a double C7=C8 bond and three unpaired electrons on atoms C7, C8, and C10, and the second with a triple C7≡C8 bond and only one unpaired electron on C10 (Fig. 5c). The first Lewis structure is supported by the high calculated spin densities of −0.31, + 0.59, and + 0.81 *e* on C7, C8, and C10, respectively, whereas the second is evidenced by the natural bond order of 2.79 for C7–C8.

The feasibility of the [2 + 2] cycloaddition is attributed to the peculiar electronic structure of the phenylethynyl radical. Schaefer and co-workers[26] revealed that although the $^2A_1$ (σ-radical) is the ground electronic state of phenylethynyl, the lowest excited π state $^2B_1$ lies only about 7 kJ mol^{-1} higher at their highest CCSD(T)/cc-pVQZ level of theory, and the energetic order of the σ- and π-radical state may even switch at different theoretical levels. For comparison, in the parent ethynyl radical, the energy difference between the ground σ and excited π states is much higher (44 kJ mol^{-1}). Although the optimized structure of phenylethynyl is slightly distorted from C_{2v} to C_s, Schaefer and co-workers used the C_{2v} symmetry species in their analysis because the energy difference between the C_{2v} and C_s structures is so small that they may not be easily distinguished experimentally and the vibrationally averaged structure will reflect C_{2v} symmetry. The energy gap between the singly-occupied a_1 highest occupied molecular orbital (HOMO) with a σ-character and the underlying doubly-occupied b_1 MO with a π-character illustrated in Fig. 5d is small. Therefore, an electron can be easily promoted between them thus enabling a versatile reactivity of phenylethynyl, where the end-on and side-on barrierless

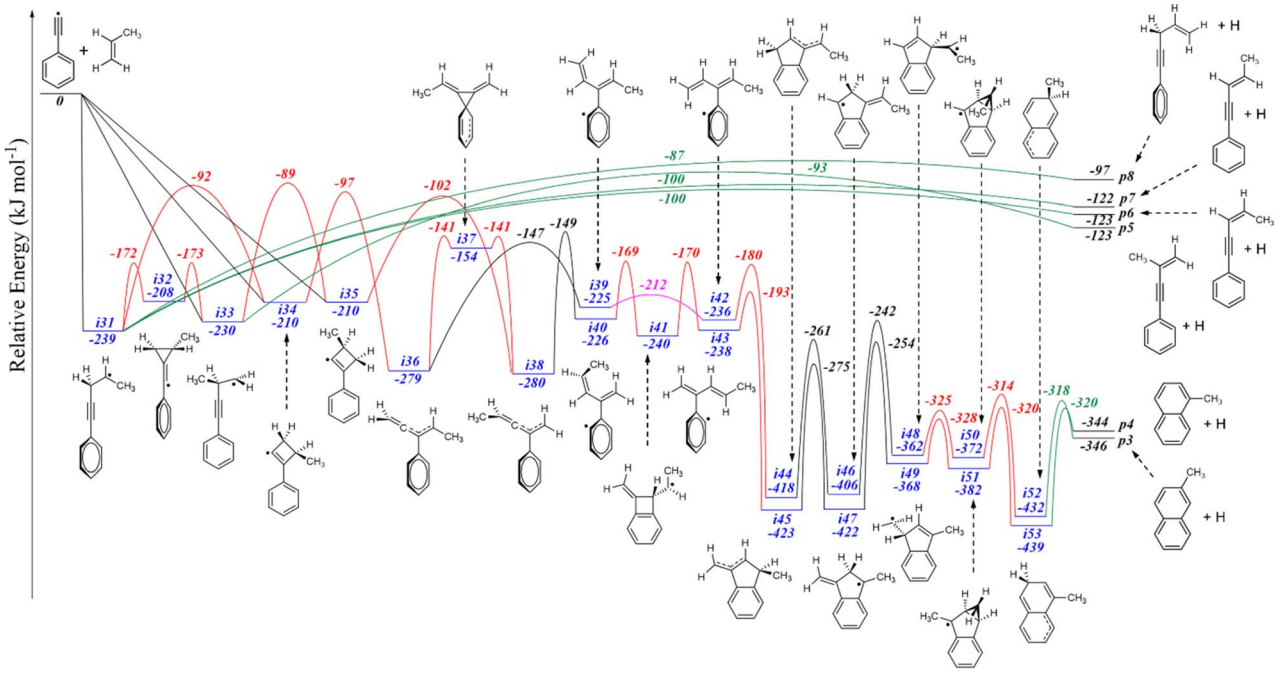

Fig. 6 Schematic potential energy surface leading to the formation of 1- and 2-methylnaphthalene ($C_{11}H_{10}$) from the reaction of the phenylethynyl radical (C_6H_5CC) with propylene (C_3H_6) calculated at the G3(MP2,CC)//ωB97X-D/6-311G(d,p) level. Hydrogen migration, bond rotation, and ring opening/closing are denoted by black, magenta, and red lines between intermediates, respectively, while exit channels to products are green. The complete surfaces are shown in SI Fig. 9–12.

Table 1 Statistical branching ratios (%) for the reaction of the phenylethynyl radical with ethylene with **i1** or **i25** as an initial intermediate at a collision energy of 20 kJ mol^{-1}

	Initial intermediate		
Product	**i1**	**i25**	**i25**[a]
p1	0.0	3.1	14.1
p2	99.8	82.7	57.0
Other[b]	0.1	14.2	28.9

[a] Transition state energies varied within potential error margins of the computational method used to assess maximum branching ratio for **p1**. [b] Other products branching ratios are detailed in the SI.

approaches of ethylene are due to its interaction with the σ and π orbitals, respectively. In the latter case, the MOs for the transformation from the initial transition state region to **i25** are shown in Fig. 5e, where the four-membered ring closure can be visualized by the carbon–carbon bond formation, ethylene fragment bond order reduction, and radical site localization on the terminal carbon of the phenylethynyl moiety. The σ–π energy gap could likely serve as a good indicator for the substituted ethynyl radical–alkene [2 + 2] cycloaddition to be plausible. It would be interesting to investigate the effect of the substituent on the ethynyl radical (*e.g.*, alkenyl *vs.* aryl) and of a side group on the aryl substituent (*e.g.*, electron-withdrawing *vs.* electron-donating) on the [2 + 2] cycloaddition reactivity. Here, we have computed the energy differences between the σ and π electronic states of methylethynyl (CH_3CC) and vinylethynyl (C_2H_3CC) using a similar level of theory as used by Schaefer and co-workers,[26] CCSD(T)/cc-pVQZ//ωB97XD. It appears that methylethynyl is similar to unsubstituted ethynyl in the sense that the π state lies significantly higher in energy than the σ state (52 kJ mol^{-1}) and hence, the effect of alkyl substitution is not expected to be substantial. Conversely, in vinylethynyl, the σ–π energy gap reduces to 28 kJ mol^{-1} and, adiabatically, at the geometries optimized for each state, the π state is slightly lower in energy than the σ state (by 1.6 kJ mol^{-1}). This result indicates that the alkenyl substitution providing the opportunity for conjugation between the π electronic systems of ethynyl and the substituent can also lower the energy of the π state and thus make the radical reactive toward [2 + 2] cycloaddition to an alkene. This consideration opens interesting new directions for future studies.

Potential energy surfaces: C_6H_5CC–C_3H_6 system

Turning to reaction (2), the experimental reaction energy of −321 ± 58 kJ mol^{-1} matches those calculated for 1- and 2-methylnaphthalene ($C_{11}H_{10}$, **p4** and **p3**, −344 and −346 kJ mol^{-1}) coupled with atomic hydrogen loss (Fig. 6). As the propylene reactant can be thought of as methyl-substituted ethylene, the reaction is initiated through similar means. Here, the phenylethynyl radical can add without barrier to the C1 or C2 carbon of propylene giving different collision complexes (**i31** and **i33**) due to the asymmetry instilled by the methyl group. Both **i31** and **i33** may emit a hydrogen atom from the attacked carbon of the side chain to form products **p6**–**p8** and **p5**, respectively, in which cyclization does not occur. The exit transition state barriers range from 137–152 kJ mol^{-1}.

Additionally, the reactants can follow the same cycloaddition entrance channel as detailed for the phenylethynyl–ethylene system to form intermediates **i34** and **i35**, where a hydrogen has been substituted by a methyl group. The isomerization barriers from **i31** to **i34** and **i33** to **i35** are a few kJ mol^{-1} higher than the barriers for H losses leading to **p5–p7** and the hydrogen atom losses are also entropically favored, suggesting that the end-on addition of propylene is not likely to lead to a second aromatic ring closure, whereas cycloaddition is the more likely entrance channel toward the formation of 1- and 2-methylnaphthalene. The route to 2-methylnaphthalene (**p3**) is initiated from collision complex **i34** and is nearly identical to reaction (1), with the methyl group acting as a spectator. The pathway to 1-methylnaphthalene (**p4**) starting from **i35** is slightly different in that instead of the bond rotation about the α–β carbon–carbon single bond of the side chain (**i39** → **i42**), a de facto bond rotation is achieved through four-membered ring closing and opening (**i40** → **i41** → **i43**).

Next, we turn to RRKM calculations to verify the most probable reaction pathways. For the initial collision complexes, statistical calculations predict only the formation of higher energy products with **i31** and **i33** as initial intermediates (Tables 2, S8 and S9); thus, the entrance channels involving **i31** and **i33** are rendered inconsequential for the formation of 1- and 2-methylnaphthalene. The two remaining routes have a crossing point through a three-membered ring complex (**i37**), but the calculated rate constants leading to **i37** are at least an order of magnitude lower than the **i36** → **i39** and **i38** → **i40** isomerization (Table S2), so it is likely that the two routes remain mostly independent. For product formation, the statistical branching ratios predict levels of up to 4% for **p3** and up to 18% for **p4** at $E_C = 20$ kJ mol^{-1} when **i34** and **i35** are the initial intermediates, respectively, indicating that the methyl group is preferred *ortho* to the adjoining benzene ring (Table 2). This is likely due to steric hindrance in the entrance channel giving preference to collision complexes where the phenyl and methyl groups are at the opposite sides of the newly formed four-membered ring (**i35**). Overall, reactions (1) and (2) highlight a unique phenylethynyl addition–cyclization–aromatization mechanism initiated by a barrierless, [2 + 2] cycloaddition leading to (substituted) aromatic molecules in which substituents can be varied by tuning the side group(s) on the secondary reactant.

Table 2 Statistical branching ratios (%) for the hydrogen atom loss channels in the reaction of the phenylethynyl radical with propylene with **i31**, **i33**, **i34**, or **i35** as initial intermediates at a collision energy of 20 kJ mol^{-1}

	Initial intermediate					
Product	**i31**	**i33**	**i34**	**i35**	**i34**[a]	**i35**[a]
p3	0.0	0.0	0.0	0.0	3.5	0.2
p4	0.0	0.0	0.0	0.9	0.3	18.3
p5	42.7	11.6	5.1	0.5	4.4	0.4
p6	11.5	42.6	19.5	1.8	16.3	1.3
p7	34.3	34.2	15.9	1.5	13.2	1.1
p8	11.5	11.6	5.4	0.5	4.4	0.4
Other[b]	0.0	0.0	54.1	94.8	57.9	78.3

[a] Transition state energies varied within potential error margins of the computational method used to assess maximum branching ratios for **p3** and **p4**. [b] Other products branching ratios are detailed in the SI.

Conclusions

Overall, our crossed molecular beam and computational study on the reaction of phenylethynyl radicals (C_6H_5CC) with two unsaturated hydrocarbons—ethylene-d_4 (C_2D_4) and propylene (C_3H_6)—uncovers the formation of naphthalene-d_4 (**p1**) and 1- and 2-methylnaphthalene (**p4**, **p3**), respectively, coupled with atomic hydrogen loss under single collision conditions. The naphthalene and methylnaphthalene formation reactions are initiated under thermal conditions without barrier through a [2 + 2] cycloaddition between the ethynyl and ethenyl moieties of each reactant forming four-membered ring collision complexes—such constrained species containing three- or four-membered rings are frequently observed on complex potential energy surfaces. Cycloaddition reactions in general are rather common—some examples being Diels–Alder,[27] nitrone–olefin,[28] and Huisgen[29] cycloaddition. However, thermal [2 + 2] cycloaddition without the use of an allene or ketene moiety is quite rare, and acetylenic radicals are not traditionally known to undergo [2 + 2] cycloaddition. Owing to the small energy gap between the singly-occupied a_1 (HOMO) with a σ-character and the underlying doubly-occupied b_1 MO with a π-character allowing a facile promotion of an electron enables a versatile reactivity of phenylethynyl, where the end-on and side-on barrierless approaches of ethylene are due to its interaction with the σ and π orbitals, respectively. The remaining reaction pathways involve ring opening and closing, bond rotation, and hydrogen shift isomerization leading eventually to aromatization and formation of the 10π aromatic naphthalene product. The routes for the ethylene and propylene reactions are similar, indicating that the methyl group on the propylene reactant acts as a spectator throughout the reaction sequence where it eventually ends up as a side group on the naphthalene product. The reactivity of ethylene and propylene with the phenylethynyl radical is different than for the similar radicals ethynyl (HCC) and 1-propynyl (CH_3CC), where the phenyl group has been replaced by a hydrogen and a methyl group, respectively. In the four cases of ethynyl–ethylene,[20] ethynyl–propylene,[21] 1-propynyl–ethylene,[30] and 1-propynyl–propylene,[31] none of the entrance channels feature a cycloaddition mechanism. The delocalized π-electrons of the phenyl ring on the phenylethynyl radical influence the reactivity of the ethynyl moiety in such a way as to stabilize the first excited π-radical state of phenylethynyl resulting in promotion of the cycloaddition mechanism. Traditionally, integrating alternate groups on the ethylene moiety, such as alkynes or alkenes, could link this mechanism to the thermal enediyne[32] and ene-yne-allene[33] cyclization reactions, respectively; however, the computations did not reveal any of those pathways. Instead, the cycloaddition framework may be expanded by incorporating different groups on the ethylene backbone, where the nature and position of the naphthalene substituent(s) can be tuned—potentially inducing chirality and atropisomerism for stereoselective

applications[34]—and ultimately advancing our fundamental understanding of carbon chemistry at its roots.

Author contributions

R. I. K. designed and supervised the experiment; S. J. G., I. A. M., C. H., Z. Y., and A. S. performed the experimental measurements; A. P.-G. synthesized the experimental precursor; W. S. supervised the precursor synthesis; S. J. G. performed the experimental data analysis; A. A. N. carried out the theoretical analysis; A. M. M. supervised the theoretical analysis; S. J. G., W. S., A. M. M., and R. I. K. wrote the paper.

Conflicts of interest

There are no conflicts to declare.

Data availability

The data that support the findings of this study are available in the article and the supplementary information (SI). Additional data are available from the corresponding authors upon request. Supplementary information: experimental methods, computational methods, comparison of H *vs.* D loss, precursor synthesis and characterization, H *vs.* D loss lab data (Fig. S1), H *vs.* D loss CM data (Fig. S2), TOF overlap (Fig. S3), additional PESs (Fig. S4–S12), NMR spectra of precursors (Fig. S13 and S14), rate constants (Tables S1 and S2), branching ratios (Tables S3–S11), molecular cartesian coordinates, supplementary references. See DOI: **https://doi.org/10.1039/d5sc05991g**.

Acknowledgements

The experimental studies at the University of Hawaii were supported by the US Department of Energy, Basic Energy Sciences DE-FG02-03ER15411. The studies at Florida International University were supported by US Department of Energy, Basic Energy Sciences DE-FG02-04ER15570. The chemical synthesis in Bochum was supported by the Deutsche Forschungsgemeinschaft (DFG, German Research Foundation) under Germany's Excellence Strategy-EXC-2033 390677874 RESOLV.

Notes and references

1 W. Lee, Y. Koo, H. Jung, S. Chang and S. Hong, *Nat. Chem.*, 2023, **15**, 1091–1099.
2 Q.-Y. Li, Y.-H. Deng, C. Cao, Y.-X. Hong, X.-R. Xue, M.-J. Zhang, Y. Ge, B. F. Abrahams and J.-P. Lang, *Angew. Chem., Int. Ed.*, 2023, **62**, e202306719.
3 D. Richter, E. Lakis and J. Piel, *Nat. Chem.*, 2023, **15**, 1422–1430.
4 B. T. Worrell, J. A. Malik and V. V. Fokin, *Science*, 2013, **340**, 457–460.
5 B.-R. Wang, Y.-B. Li, Q. Zhang, D. Gao, P. Tian, Q. Li and L. Yin, *Nat. Commun.*, 2023, **14**, 4688.
6 A. Grirrane, H. Garcia, A. Corma and E. Álvarez, *ACS Catal.*, 2011, **1**, 1647–1653.
7 G. W. Goodall and W. Hayes, *Chem. Soc. Rev.*, 2006, **35**, 280–312.
8 G. Delaittre, N. K. Guimard and C. Barner-Kowollik, *Acc. Chem. Res.*, 2015, **48**, 1296–1307.
9 P. Ding, S. Wang, C. Mattioli, Z. Li, G. Shi, Y. Sun, A. Gourdon, L. Kantorovich, F. Besenbacher, F. Rosei and M. Yu, *Nat. Commun.*, 2023, **14**, 6075.
10 X. Zhang, A. Fan and C. S. Foote, *J. Org. Chem.*, 1996, **61**, 5456–5461.
11 K. C. Nicolaou, S. A. Snyder, T. Montagnon and G. Vassilikogiannakis, *Angew. Chem., Int. Ed.*, 2002, **41**, 1668–1698.
12 R. Hoffmann and R. B. Woodward, *J. Am. Chem. Soc.*, 1965, **87**, 2046–2048.
13 D. Sarkar, N. Bera and S. Ghosh, *Eur. J. Org Chem.*, 2020, **2020**, 1310–1326.
14 D. Didier and F. Reiners, *Chem. Rec.*, 2021, **21**, 1144–1160.
15 M. W. Smith and P. S. Baran, *Science*, 2015, **349**, 925–926.
16 B. Alcaide, P. Almendros and C. Aragoncillo, *Chem. Soc. Rev.*, 2010, **39**, 783–816.
17 M. A. Ischay, M. E. Anzovino, J. Du and T. P. Yoon, *J. Am. Chem. Soc.*, 2008, **130**, 12886–12887.
18 K. L. Hurni and K. M. Baines, *Chem. Commun.*, 2011, **47**, 8382–8384.
19 S. J. Goettl, Z. Yang, S. Kollotzek, D. Paul, R. I. Kaiser, A. Somani, A. Portela-Gonzalez, W. Sander, A. A. Nikolayev, V. N. Azyazov and A. M. Mebel, *J. Phys. Chem. A*, 2023, **127**, 5723–5733.
20 F. Zhang, Y. S. Kim, R. I. Kaiser, S. P. Krishtal and A. M. Mebel, *J. Phys. Chem. A*, 2009, **113**, 11167–11173.
21 S. J. Goettl, C. He, D. Paul, A. A. Nikolayev, V. N. Azyazov, A. M. Mebel and R. I. Kaiser, *J. Phys. Chem. A*, 2022, **126**, 1889–1898.
22 R. I. Kaiser, C. Ochsenfeld, D. Stranges, M. Head-Gordon and Y. T. Lee, *Faraday Discuss.*, 1998, **109**, 183–204.
23 J. Laskin and C. Lifshitz, *J. Mass Spectrom.*, 2001, **36**, 459–478.
24 W. B. Miller, S. A. Safron and D. R. Herschbach, *Discuss. Faraday Soc.*, 1967, **44**, 108–122.
25 R. A. Marcus, *J. Chem. Phys.*, 1952, **20**, 359–364.
26 R. K. Sreeruttun, P. Ramasami, C. S. Wannere, A. C. Simmonett and H. F. Schaefer, *J. Phys. Chem. A*, 2008, **112**, 2838–2845.
27 O. Diels and K. Alder, *Adv. Cycloaddit.*, 1928, **460**, 98–122.
28 N. A. LeBel, M. E. Post and J. J. Whang, *J. Am. Chem. Soc.*, 1964, **86**, 3759–3767.
29 R. Huisgen, *Proc. Chem. Soc.*, 1961, 357–369.
30 C. He, L. Zhao, A. M. Thomas, G. R. Galimova, A. M. Mebel and R. I. Kaiser, *Phys. Chem. Chem. Phys.*, 2019, **21**, 22308–22319.
31 I. A. Medvedkov, A. A. Nikolayev, C. He, Z. Yang, A. M. Mebel and R. I. Kaiser, *Mol. Phys.*, 2024, **122**, e2234509.
32 K. C. Nicolaou and W.-M. Dai, *Angew. Chem., Int. Ed.*, 1991, **30**, 1387–1416.
33 R. F. Cunico and S. K. Nair, *Tetrahedron Lett.*, 1997, **38**, 25–28.
34 C. B. Roos, C.-H. Chiang, L. A. M. Murray, D. Yang, L. Schulert and A. R. H. Narayan, *Chem. Rev.*, 2023, **123**, 10641–10727.